T-type L-2L De-Embedding Method for On-Wafer T-model Transmission Line Network

M. Seyedi
School of ECE, College of Eng
University of Tehran
Tehran, Iran
Milad.seyedi@ut.ac.ir

N. Masoumi
School of ECE, College of Eng
University of Tehran
Tehran, Iran
Nmasoumi@ut.ac.ir

S. Sheikhaei
School of ECE, College of Eng
University of Tehran
Tehran, Iran
Sheikhaei@ut.ac.ir

***Abstract*— This paper presents an extensive evaluation for a new type of the L–2L de-embedding method applied to on-chip de-embedding. We derive analytical formulas to discuss and verify the accuracy of the improved and extended method called the T-type L-2L de-embedding. The case study structure to apply the new method consists of a microstrip line combined with two left- and right-side pads. For the simulation of the structures, HFSS 3D electromagnetic (EM) simulator is used. The results show that the T-type L-2L exhibits better accuracy compared with the other on-wafer de-embedding methods for a device under test (DUT).**

***Key words*— L-2L, de-embedding, IC pad, Microstrip line, S-Parameters, Device Under Test (DUT).**

I. Introduction

To obtain the actual characteristics of a DUT, the parasitic effects of the fixtures and on-wafer interconnects must be removed using a de-embedding method. Today, for reliable measurements of circuits in the silicon-integrated technology for millimeter and sub-millimeter wave frequencies no solutions are provided except the de-embedding methods [1]. To extract S-parameters of a DUT, the de-embedding methods generate emendations of the passive structures and active circuits in the millimeter and sub-millimeter frequencies range. Thus, a de-embedding step must be performed to derive the intrinsic parameters of the DUT.

The frequency de-embedding methods are classified into three types according to their de-embedding performance [2], Cascaded Matrix Based Model (CMBM), Lumped Equivalent Circuit Model (LECM), and Cascaded Matrix with Lumped Equivalent Models (CMLEM). In the CMBM, the fixtures and interconnect parasitics are calculated differently, and the mathematical operations on each test structure are performed to obtain the DUT characterization. These methods are accurate in de-embed large-scale structures (compared to the wavelengths of $L_{max} > 0.1\lambda$) and long transmission lines. For this class of de-embedding methods, the standard Thru-Reflect-Line (TRL) [3], Short-Open-Load-Thru (SOLT) [4], and 2x-Thru [5] de-embedding methods can be mentioned. Using this class of methods at the IC level is costly due to space limitations [1]. The second and third classes of de-embedding methods are suitable for IC-level structures and are called wafer-level de-embedding [1]. These methods are used to de-embed the DUT with lengths very small compared to the considered wavelengths. The LECM methods are very simple compared to the other de-embedding methods and are utilized for low-frequency ranges. The Short (S) [6] and Open-Short (OS) methods [7] are among this categorization. The CMLEM methods cost more than LECM methods however they cover a much higher frequency range. For the CMLEM class, L_iL_j [8] and the π-type L-2L [9-13] de-embedding methods can be mentioned. The method is revised to decrease its sensitivity to measurement noise for the on-chip de-embedding [9]. The performance of via-less interconnect with different dielectric materials on glass was evaluated in [10]. The [11] validates π-type L-2L de-embedding for TMV RF characteristics up to 50GHz with varying TMV structures. In [12] utilized the L-2L de-embedding method to enhance signal integrity for the flip-chip structure on a heterogeneous silicon interposer surface. L-2L de-embedding was used for characterization in the 40-170 GHz frequency range. However, the π-type L-2L method is compatible with the RAW device (not de-embedded), which is considered a π-model two-port network. The authors in [13] have presented the methods to apply the L-2L method based on the model of the pads (fixtures), π-type, T-type, and double T-type. The methodologies of [13] to apply L-2L are complicated. In this paper, we propose a simple L-2L de-embedding method proportionate to the RAW devices, which is considered as a T-model network. We call the method, the T-type L-2L method. The validity of this method is compared with the π-type L-2L method and ANSYS HFSS simulated DUT.

The structure of this paper is followed as: The detail of the RAW device is discussed in Section II. Section III describes the conventional wafer-level de-embedding. The implementation and methodology of T-type L-2L de-embedding are discussed in Section IV. Section V presents the final conclusion.

II. Structure Details

The largest dimensions of discontinuity structures to employ the on-wafer de-embedding methods must be much smaller than the considered wavelength [1]; this means that these structures can be modeled as lumped elements. The rule of thumb from empirical tests states that a lumped element circuit representation holds true as long as the wavelength λ at the highest frequency f of interest remains very large to the structure's physical size *Length* (e.g., *Length* < λ/20). The wavelength in a specific medium of electromagnetic wave is related to its frequency, effective permittivity of the medium ε_{eff}, and the free-space light velocity $c_0 \approx 2.998 \times 10^8\ m/s$ by the well-known formula

$$\lambda = \frac{c_0}{f\sqrt{\varepsilon_{eff}}} \quad (1)$$

A material with a high permittivity polarizes more in response to an applied electric field than a material with a low permittivity, thereby storing more energy in the material. The difference is that ε_{eff} is measured in a non-homogeneous material (a mixture of different materials having different relative permittivities ε_r). Because in the microstrip

configuration, the bottom layer is dielectric and the top layer is air, the effective permittivity of the microstrip line structure is obtained from [14],

$$\varepsilon_{eff} = \begin{cases} \frac{\varepsilon_r+1}{2} + \frac{\varepsilon_r-1}{2}\left[\left(1+12\left(\frac{H}{W}\right)\right)^{-\frac{1}{2}} + 0.04\left(1-\left(\frac{H}{W}\right)\right)^2\right] & if\ \left(\frac{H}{W}\right) < 1 \\ \frac{\varepsilon_r+1}{2} + \frac{\varepsilon_r-1}{2}\left[\left(1+12\left(\frac{H}{W}\right)\right)^{-\frac{1}{2}}\right] & if\ \left(\frac{H}{W}\right) > 1 \end{cases} \quad (2)$$

We consider a maximum frequency of interest 60 GHz, so according to (1) the wavelength value would be 2.935 mm. The largest dimensions of discontinuity structures must be less than $147\mu m$.

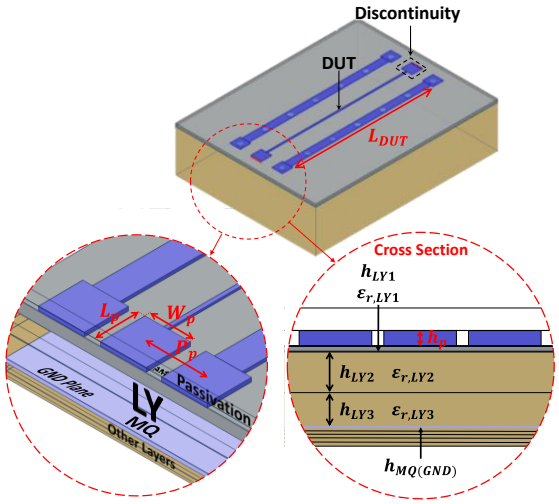

Fig. 1. Proposed structure with microstrip line, left-, and right-pads.

Fig. 1 shows the structure called RAW device (not de-embedded), where a transmission line/microstrip line of length L_{DUT} is considered as a DUT. The design parameters of the structure are shown in Table 1, the parameters are based on Fig. 1. Also, the dielectric substrate is made of silicon. For the simulation of the structures, HFSS 3D electromagnetic (EM) simulator, which is very accurate for comparison with real measurements, is employed.

TABLE I
MATERIAL PARAMETERS AND DIMENSIONS

PARAMETER	VALUE	PARAMETER	VALUE
Pad width (W_p)	75 µm	LY1 height (h_{LY1})	0.12 µm
Pad pitch (P_p)	150 µm	$\varepsilon_{r,LY1}$	4.2721
Pad height (h_p)	4 µm	LY2 height (h_{LY2})	5.4 µm
Pad length (L_p)	75 µm	$\varepsilon_{r,LY2}$	4.1219
DUT length (L_{DUT})	1 mm	LY3 height (h_{LY3})	4.0085 µm
MQ height ($h_{MQ(GND)}$)	0.6 µm	$\varepsilon_{r,LY3}$	4.1428

In this structure, we want to de-embed the scattering parameters (S-parameters) of the microstrip transmission line with a length of 1mm.

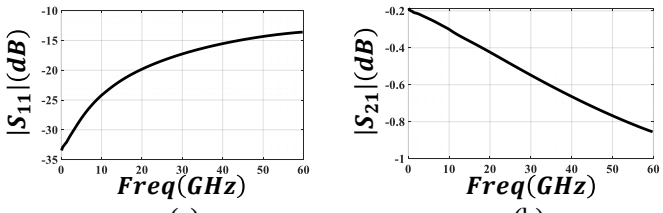

Fig. 2. the S-parameters of the RAW device, (a) amplitude of the S_{11}, (b) amplitude of the S_{21}.

In this paper, we call the 1mm microstrip transmission line the device under test (DUT), as shown in Fig. 1. Fig. 2 represents the scattering parameters of the RAW device shown in Fig. 1, the value of S_{11} and S_{21} in the frequency range of 0 to 60 GHz is from -35 to -13 dB and -0.21 to -0.84 dB, respectively.

III. ANALYZING THE ON-WAFER DE-EMBEDDING METHOD

A. L_iL_j De-embedding Method

To employ the L_iL_j de-embedding method, the measurement of two test structures consists of transmission lines with left- and right-pads is required. The length of one must be larger than the other. We consider 1.5 mm for the larger length and 0.5 mm for the smaller length. The Fig. 3 indicate the test structure of the method. The only condition that must be met is that the test structures must be symmetrical, meaning that the left- and right-pad are assumed to be the same.

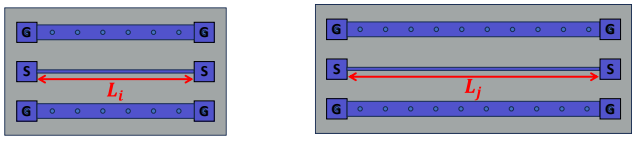

Fig. 3. Test structures required for L_iL_j de-embedding method, (a) the structure with the smaller transmission line (T_{meas-L_i}), (b) the structure with the longer transmission line (T_{meas-L_j}).

The pads are modeled as a shunt admittance, $Y = j\omega C$. Through use of network theory, the transmission matrix of a structure including a transmission line of length L_i and its pads (T_{meas-L_i}), can be represented as the following cascade of transmission matrices:

$$T_{meas-L_i} = T_{left-p} \cdot T_{L_i} \cdot T_{right-p} \quad (3)$$

where, T_{L_i} represents the transmission matrix of the line with the length of L_i, T_{left-p} represents the transmission matrix of the left-pad, and $T_{right-p}$ represents the transmission matrix of the right-pad. The conversion between T-parameters and S-parameters is represented in [16].

After measuring both test structures, the T-matrix of the longer transmission line (T_{meas-L_j}) can be right multiplied by the inverted T-matrix of the shorter transmission line (T_{meas-L_i}) to yield the following equation:

$$T_h = T_{meas-L_j} \cdot T^{-1}_{meas-L_i} = T_{left-p} \cdot T_{L_j-L_i} \cdot T^{-1}_{left-p} \quad (4)$$

where, $T_{L_j-L_i}$ is the transmission matrix of a transmission line of length $L_j - L_i$.

Using this property, the effect of the pads can be removed, yielding the admittance matrix of a transmission line of length $L_j - L_i$:

$$Y_{L_j-L_i} = \frac{Y_h + Sawp(Y_h)}{2} \quad (5)$$

where, Y_h is the converted T_h matrix to the admittance matrix and the $Sawp(Y_h)$ represent swapped the arrays of Y_h matrix (see equation (6)) [16].

$$Sawp\left(\begin{bmatrix} y_{11} & y_{12} \\ y_{21} & y_{22} \end{bmatrix}\right) = \begin{bmatrix} y_{22} & y_{21} \\ y_{12} & y_{11} \end{bmatrix} \quad (6)$$

where, the y_{11}, y_{12}, y_{21}, and y_{22}represent the arrays of Y_h matrix.

Fig. 4 indicates the scattering parameters of the DUT. The accuracy of this method for less than 0.3dB error to de-embedding the S-parameters DUT compared to the individually simulated one is limited to the frequency range of up to 30 GHz.

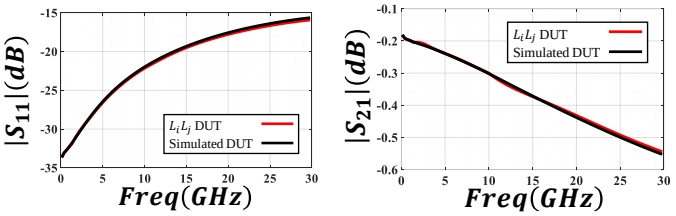

(a) (b)

Fig. 4. De-embedded S-parameters of DUT using L_iL_j method, (a) amplitude of the S_{11}, (b) amplitude of the S_{21}.

D. π-type L-2L De-embedding Method

Similar to the L_iL_j method, the π-type L-2L de-embedding method also requires the measurement of two test structures consists of transmission lines with left- and right-pad [11-13]. However, in this method, if the first transmission is of length L, the second transmission line must be of the length $2L$. In this method similar to L_iL_j the test structures must be symmetrical, meaning that the left- and right-pads are assumed to be the same. Fig. 3(a) and (b) shows the de-embedding test structures. To analyze this method, we consider 2 mm for the larger length ($L_j = 2L = 2\ mm$) and 1 mm for the smaller length ($L_i = L = 1\ mm$). The test structures are decoupled into a series cascade of three two-port networks, including the left- and right-side pads, together with their intrinsic transmission line, as shown by the following equations,

$$T_{meas-L} = T_{left-p} \cdot T_L \cdot T_{right-p} \quad (7)$$

$$T_{meas-2L} = T_{left-p} \cdot T_{2L} \cdot T_{right-p} \quad (8)$$

where T_L and T_{2L} represent the transmission matrices of the lines of the lengths L and $2L$, respectively. Also, T_{left-p} and $T_{right-p}$ show the transmission matrices of the left- and right-pad, respectively. If the length of the intrinsic transmission lines is properly designed as $L_j = 2L_i$, the multiplication of the T_{left-p} to the $T_{right-p}$ matrices can be extracted using the following equation.

$$T_{th} = T_{meas-L} \cdot T_{meas-2L}^{-1} \cdot T_{meas-L} = T_{left-p} \cdot T_{right-p} \quad (9)$$

To obtain T_{left-p} and $T_{right-p}$ from the T_{th} matrix, the two-port network of the RAW device is considered as a π-model network, as shown in Fig. 5. Additionally, the left-pad is modeled as a shunt admittance, $Y_{sh} = G + j\omega C$, followed by a series impedance, $Z_{ser} = R + j\omega L$ and similarly, the right-pad is modeled as a series impedance, $Z_{ser} = R + j\omega L$, followed by a shunt admittance, $Y_{sh} = G + j\omega C$. The concept of choosing the name of the π-type L-2L de-embedding method is based on this condition. Therefore, T_{th} represents the transmission matrix of a π-model two-port network, which denoted by $T_{\pi-th}$. Therefore, T_{left-p} and $T_{right-p}$ are calculated out from the $T_{\pi-th}$ matrix using the following equations [11-13]

$$T_{left-p} = \begin{bmatrix} 1 & \frac{B_{\pi-th}}{2} \\ \frac{C_{\pi-th}}{\left(1+\frac{(A_{\pi-th}+D_{\pi-th})}{2}\right)} & \frac{1+B_{\pi-th}C_{\pi-th}}{2\left(1+\frac{(A_{\pi-th}+D_{\pi-th})}{2}\right)} \end{bmatrix} \quad (10)$$

$$T_{right-p} = \begin{bmatrix} \frac{1+B_{\pi-th}C_{\pi-th}}{2\left(1+\frac{(A_{\pi-th}+D_{\pi-th})}{2}\right)} & \frac{B_{\pi-th}}{2} \\ \frac{C_{\pi-th}}{\left(1+\frac{(A_{\pi-th}+D_{\pi-th})}{2}\right)} & 1 \end{bmatrix} \quad (11)$$

where, $A_{\pi-th}$, $B_{\pi-th}$, $C_{\pi-th}$, and $D_{\pi-th}$ represent the arrays of the $T_{\pi-th}$ matrix ($T_{\pi-th} = T_{th}$).

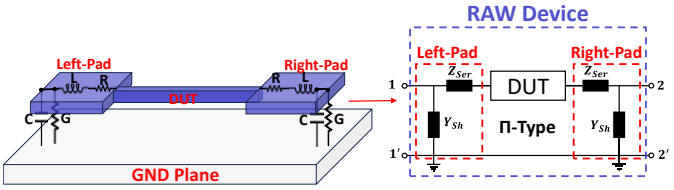

Fig. 5. π-model tow-port RAW device network.

After obtaining T_{left-p} and $T_{right-p}$, the transmission matrix of the DUT can be extracted using the following equation,

$$T_{DUT} = T_{left-p}^{-1} \cdot T_{RAW} \cdot T_{right-p}^{-1} \quad (12)$$

where T_{DUT} and T_{RAW} represent the transmission matrices of the DUT the RAW device, respectively. Fig. 7 shows the de-embedded S-parameters of the DUT using the π-type L-2L de-embedding method. This method exhibits a good accuracy in de-embedding the DUT compared to the simulation results, which covers the whole frequency range up to 60 GHz.

The parasitic elements of the pads such as resistance, inductance, capacitance, and conductance using this method can be calculated from the equations (13) and (14) [12]. Fig. 8 indicates the parasitic elements of the pads.

$$Z_{ser} = \frac{B_{\pi-th}}{2}\begin{cases} R = Re\{Z_{ser}\} \\ L = \frac{Im\{Z_{ser}\}}{2\pi f} \end{cases} \quad (13)$$

$$Y_{sh} = \frac{A_{\pi-th}-1}{B_{\pi-th}}\begin{cases} G = Re\{Y_{sh}\} \\ C = \frac{Im\{Y_{sh}\}}{2\pi f} \end{cases} \quad (14)$$

IV. *T-TYPE $L-2L$ DE-EMBEDDING METHOD*

The main concept of the T-type L-2L de-embedding method is similar to the π-type L-2L de-embedding method, which is based on the equations (7), (8), and (9). However, in this method, to obtain T_{left-p} and $T_{right-p}$ from (9), the two-port network of the RAW device is considered as a T-model network, as shown in Fig. 6. Additionally, the left-pad is modeled as a series impedance, $Z_{ser} = R + j\omega L$, followed by a shunt admittance, $Y_{sh} = G + j\omega C$ and similarly, the right-pad is modeled as a shunt admittance, $Y_{sh} = G + j\omega C$, followed by a series impedance, $Z_{ser} = R + j\omega L$. Therefore, T_{th} represents the transmission matrix of a T-model two-port network, which we denote T_{T-th}. Therefore, T_{left-p} and $T_{right-p}$ are calculated out from (9) using the following equations,

$$T_{left-p} = \begin{bmatrix} \frac{1+B_{T-th}C_{T-th}}{2+A_{T-th}+D_{T-th}} & \frac{1+B_{T-th}C_{T-th}}{2+A_{T-th}+D_{T-th}} \\ \frac{C_{T-th}}{2} & 1 \end{bmatrix} \quad (15)$$

$$T_{right-p} = \begin{bmatrix} 1 & \frac{1+B_{T-th}C_{T-th}}{2+A_{T-th}+D_{T-th}} \\ \frac{C_{T-th}}{2} & \frac{1+B_{T-th}C_{T-th}}{2+A_{T-th}+D_{T-th}} \end{bmatrix} \quad (16)$$

where, A_{T-th}, B_{T-th}, C_{T-th}, and D_{T-th} represent the arrays of the T_{T-th} matrix ($T_{T-th} = T_{th}$).

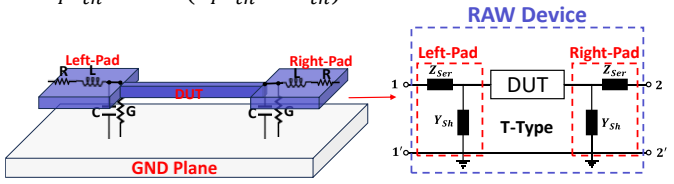

Fig. 6. T-type tow-port RAW device network.

Similar to the π-type L-2L method, after obtaining T_{left-p} and $T_{right-p}$, the transmission matrix of the DUT can be

extracted using (12). Fig. 7 shows the de-embedded S-parameters of the DUT using the T-type L-2L de-embedding method. Fig. 8 demonstrates that this method outperforms the π-type L-2L method in accuracy when compared to simulation results for the DUT, serving as reference data. Both methods cover the whole frequency range up to 60 GHz.

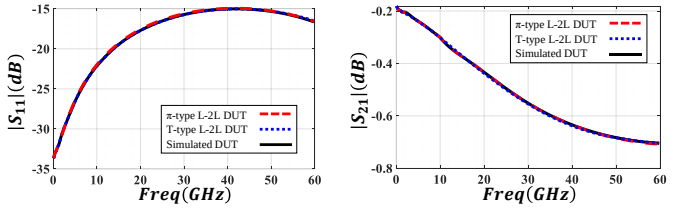

Fig. 7. De-embedded S-parameters of DUT using L − 2L method, (a) amplitude of the S_{11}, (b) amplitude of the S_{21}.

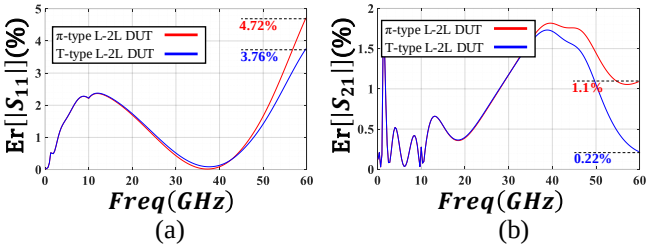

Fig. 8. Error of De-embedded DUT S-parameters compared to simulation, (a) Error of the S_{11}, (b) Error of the S_{21}.

Fig. 9 indicates the extracted parasitic elements of the pads using the T-type method, which is compared to the π-type method. The parasitic elements of pads can be calculated from the following equations,

$$Z_{ser} = \frac{A_{T-th}-1}{C_{T-th}} \begin{cases} R = Re\{Z_{ser}\} \\ L = \frac{Im\{Z_{ser}\}}{2\pi f} \end{cases} \quad (17)$$

$$Y_{sh} = \frac{C_{T-th}}{2} \begin{cases} G = Re\{Y_{sh}\} \\ C = \frac{Im\{Y_{sh}\}}{2\pi f} \end{cases} \quad (18)$$

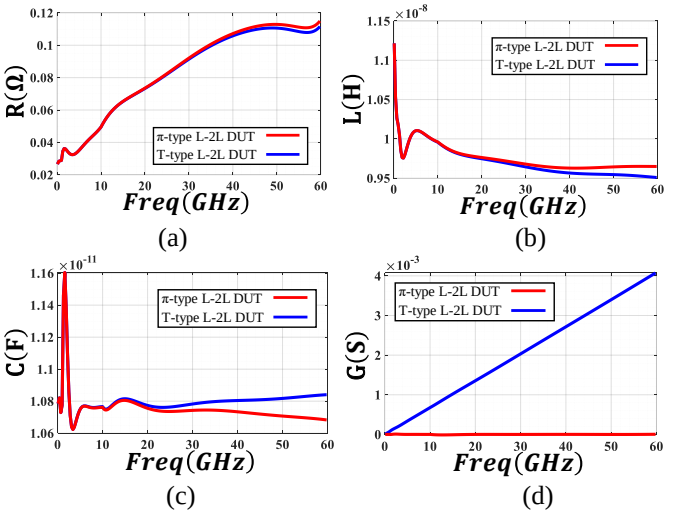

Fig. 9. De-embedded parasitics of the pads using L − 2L method, (a) resistance, (b) inductance, (c) capacitance, (d) conductance.

V. Conclusion

We have performed an extensive evaluation of the de-embedding methods for on-wafer structures and addressed the accuracy of the conventional de-embedding methods. We proposed the new T-type L-2L de-embedding method. It was proven that this method is accurate enough compared to the reference data obtained from the simulation results of the DUT, and exhibits a better accuracy compared to the conventional π-type L-2L de-embedding in the mm-wave range. The acceptable accuracy of L_iL_j is limited to 30GHz. It was shown that the accuracy of the proposed T-type L-2L method covers the whole frequency range up to 60 GHz with less than 0.3 dB error.

References

[1] Lourandakis, Errikos. "On-Wafer Microwave Measurements and De-Embedding". Artech House, Norwood, 2016.

[2] Velayudhan, Vipin. “Vectorial measurement methods for millimeter wave integrated circuits.” (2016).

[3] L. Galatro, A. Pawlak, M. Schroter and M. Spirito, "Capacitively Loaded Inverted CPWs for Distributed TRL-Based De-Embedding at (Sub) mm-Waves," in *IEEE Transactions on Microwave Theory and Techniques*, vol. 65, no. 12, pp. 4914-4924, Dec. 2017.

[4] R. A. Ginley, "Establishing traceability for SOLT calibration kits," 2017 *90th ARFTG Microwave Measurement Symposium (ARFTG)*, 2017, pp. 1-4.

[5] "IEEE Standard for Electrical Characterization of Printed Circuit Board and Related Interconnects at Frequencies up to 50 GHz," in IEEE Std 370-2020 , vol., no., pp.1-147, 8 Jan. 2021.

[6] K. T. M. Shafi, V. Baipadi and V. Vanukuru, "Layout Optimization of Short De-embedding Structure for Accurate On-Chip Inductor Characterization," 2021 IEEE 20th Topical Meeting on Silicon Monolithic Integrated Circuits in RF Systems (SiRF), San Diego, CA, USA, 2021, pp. 31-33, doi: 10.1109/SiRF51851.2021.9383413.

[7] C. Esposito et al., "Extending the Open-Short de-embedding frequency via metal-l on-wafer calibration approaches," 2022 99th ARFTG Microwave Measurement Conference (ARFTG), Denver, CO, USA, 2022, pp. 1-4, doi: 10.1109/ARFTG54656.2022.9896529.

[8] N. Erickson, K. Shringarpure, J. Fan, B. Achkir, S. Pan and C. Hwang, "De-embedding techniques for transmission lines: An exploration, review, and proposal," 2013 IEEE International Symposium on Electromagnetic Compatibility, 2013, pp. 840-845.

[9] N. Erickson, B. Achkir and J. Fan, "Revised L–2L Method for On-Chip De-Embedding," in IEEE Transactions on Electromagnetic Compatibility, vol. 61, no. 1, pp. 209-216, Feb. 2019.

[10] L. N. V. Kumar et al., "Demonstration and Comparison of Vertical Via-less Interconnects in Laminated Glass Panels from 40-170 GHz," 2022 IEEE 72nd Electronic Components and Technology Conference (ECTC), San Diego, CA, USA, 2022, pp. 2281-2286, doi: 10.1109/ECTC51906.2022.00360.

[11] L. N. V. Kumar et al., "Demonstration and Comparison of Vertical Via-less Interconnects in Laminated Glass Panels from 40-170 GHz," 2022 IEEE 72nd Electronic Components and Technology Conference (ECTC), San Diego, CA, USA, 2022, pp. 2281-2286, doi: 10.1109/ECTC51906.2022.00360.

[12] P. Namaki, N. Masoumi, M. Seyedi and M. -R. Nezhad-Ahmadi, "An Extended L–2L De-Embedding Method for Modeling and Low Return-Loss Transition of Millimeter Wave Signal Through Silicon Interposer," in IEEE Transactions on Electromagnetic Compatibility, doi: 10.1109/TEMC.2023.3311377. 2023.

[13] S. Kawai, K. K. Tokgoz, K. Okada and A. Matsuzawa, "L-2L de-embedding method with double-T-type PAD model for millimeter-wave amplifier design," 2015 IEEE 15th Topical Meeting on Silicon Monolithic Integrated Circuits in RF Systems, San Diego, CA, USA, 2015, pp. 43-45.

[14] Z. Zhou and K. L. Melde, "A Comprehensive Technique to Determine the Broadband Physically Consistent Material Characteristics of Microstrip Lines," in IEEE Transactions on Microwave Theory and Techniques, vol. 58, no. 1, pp. 185-194, Jan. 2010.